Available online at www.sciencedirect.com
ScienceDirect
Journal of Power Sources 181 (2008) 214–227
JOURNAL OF POWER SOURCES
www.elsevier.com/locate/jpowsour

The effect of the parasitic current on the Direct Ethanol PEM Fuel Cell Operation

G.M. Andreadis, A.K.M. Podias, P.E. Tsiakaras *

Department of Mechanical and Industrial Engineering, School of Engineering, University of Thessaly, Pedion Areos, 383 34 Volos, Greece

Received 29 September 2007; received in revised form 20 January 2008; accepted 21 January 2008
Available online 7 February 2008

Abstract

In the present work the effect of the parasitic or leakage current, I_p, which is the result of the ethanol crossover through the polymer electrolyte membrane (PEM) from the anode to the cathode side of the cell, on both the cathode activation overpotential and the fuel cell operation is investigated. A one-dimensional (1-D), isothermal mathematical model is developed in order to describe the operation of a Direct Ethanol PEM Fuel Cell (DE-PEMFC) in steady state. The equations used describe the mass transport of both ethanol and humidified oxygen at the anode and the cathode compartment of the cell respectively. The mathematical model is validated against experimental data and a relatively good agreement between the model predictions and the experimental results is found. The direct correlation that exists between the ethanol crossover rate and the parasitic current formation is graphically depicted. Moreover, when the parasitic current is enabled and disabled, the calculation of the cathode activation overpotential shows that the mixed overpotential for a DE-PEMFC poses a serious problem hindering the fuel cell operation. According to the model results, the parasitic current is greater at low current density values due to the greater amounts of the crossovered ethanol. Finally, the effect of both the oxygen feed concentration and the parasitic current formation on the fuel cell operation is also presented and discussed.

Keywords: Direct Ethanol PEM Fuel Cell; Mathematical modeling; Mixed overpotential; Parasitic current

1. Introduction

Direct Ethanol Proton Exchange Membrane Fuel Cells (DE-PEMFCs) are promising candidates as power sources especially at small-scale applications. The last decade polymer electrolyte membrane fuel cells (PEMFCs) directly fed by ethanol have been receiving more and more attention, due to their advantages [1]. However, there are some challenges such as high anode activation overpotential values, fuel crossover from the anode to the cathode through the electrolyte membrane and mixed overpotential at the cathode compartment of the cell that should be overcome. Over the last years, several experimental works [2–18] have been devoted to the direct use of ethanol in fuel cells (DEFCs). Almost all the above-mentioned scientific works deal with the problem of ethanol electro-oxidation kinetics at the anode compartment, and the research conducted in order more effective catalysts to be found. However, due to the fact that for the complete ethanol electro-oxidation 12 electrons must be exchanged, it makes the oxidation kinetics inherently slower for a DE-PEMFC in contrast to hydrogen PEMFC. According to the literature, PtSn/C and PtRu/C catalysts possess substantially higher intrinsic activity than pure platinum among the already tested electrocatalysts [1,2,19]. Moreover, it seems to be an optimum Pt:Ru or Pt:Sn atomic ratio leading to more effective ethanol electro-oxidation, however there is no concurrence between the scientists, which is this ratio [19].

Mathematical modeling is essential for the development of fuel cells because it allows a better comprehension of the fuel cell's design, operating parameters effect on performance, durability and operation. Many theoretical works concerning the use of methanol in PEMFCs can be found in the literature [20–35]. However, there are only few dedicated to DE-PEMFCs [36–38].

In the present investigation a one-dimensional (1-D), steady-state and isothermal mathematical model, written in FORTRAN language, has been appropriately developed with the purpose to investigate the parasitic current formation and its effect on the

* Corresponding author. Tel.: +30 24210 74065; fax: +30 24210 74050.
E-mail address: tsiak@mie.uth.gr (P.E. Tsiakaras).

0378-7753/$ – see front matter © 2008 Elsevier B.V. All rights reserved.
doi:10.1016/j.jpowsour.2008.01.060

Nomenclature

$A_v i_{o,ref}$ anode reference exchange current density times area
$A_v i^{O_2}_{o,ref}$ cathode reference exchange current density times area
$C_{F,EtOH}$ ethanol feed concentration (mol L^{-1})
C^{ref}_{EtOH} reference ethanol concentration (mol L^{-1})
C_{F,O_2} oxygen feed concentration (mol cm^{-3})
$C^{ref}_{O_2}$ reference oxygen concentration (mol cm^{-3})
D_{EtOH-H_2O} diffusion of ethanol to water ($cm^2\ s^{-1}$)
$D^{d,eff}_{EtOH}$ ethanol effective diffusion coefficient through the anode diffusion layer ($cm^2\ s^{-1}$)
$D^{c,eff}_{EtOH}$ ethanol effective diffusion coefficient through the anode catalyst layer ($cm^2\ s^{-1}$)
D^{m}_{EtOH} ethanol diffusion coefficient through PEM ($cm^2\ s^{-1}$)
$D^{d,eff}_{O_2}$ oxygen effective diffusion coefficient through the cathode diffusion layer ($cm^2\ s^{-1}$)
$D^{c,eff}_{O_2}$ oxygen effective diffusion coefficient through the cathode catalyst layer ($cm^2\ s^{-1}$)
E°_{H} thermo-neutral potential corresponding to ethanol's HHV
E° theoretical potential (Gibbs potential)
E^{Nernst} Nernst potential
F Faraday's constant (96,484 C mol^{-1})
I cell current density (A cm^{-2})
I_p parasitic current density (A cm^{-2})
i protonic current density (A cm^{-2})
$I_{lim,i}$ limiting current density due to each species (A cm^{-2})
K_m protonic conductivity of ionomer (S cm^{-1})
K^{eff}_m effective protonic conductivity in catalyst layer
K_s electronic conductivity of solid phase (Pt-Ru/C)
K^{eff}_s effective conductivity of solid phase in catalyst layer
l^{d}_{an} anode diffusion layer thickness (cm)
l^{c}_{an} anode catalyst layer thickness (cm)
l_m PEM thickness (cm)
l^{d}_{cath} cathode diffusion layer thickness (cm)
l^{c}_{cath} cathode catalyst layer thickness (cm)
N_{EtOH} local ethanol flux in catalyst layer (mol $cm^{-2}\ s^{-1}$)
N^{d}_{EtOH} ethanol flux through the diffusion layer (mol $cm^{-2}\ s^{-1}$)
N^{m}_{EtOH} ethanol flux through PEM (mol $cm^2\ s^{-1}$)
N_{diff} water flux due to the diffusion mechanism in PEM (mol $cm^{-2}\ s^{-1}$)
$N_{electrdrag}$ water flux due to the electro-osmotic drag
N_{d,H_2O} water flux through the diffusion layer (mol $cm^{-2}\ s^{-1}$)
$N^{m}_{H_2O}$ water flux through PEM (mol $cm^{-2}\ s^{-1}$)
$N^{d}_{O_2}$ oxygen flux through the cathode diffusion layer (mol $cm^{-2}\ s^{-1}$)
$N^{d,cath}_{H_2O}$ water flux through the cathode diffusion layer
$N^{c,cath}_{H_2O}$ water flux through the cathode catalyst layer
$n_{H_2O/drag}$ electro-osmotic drag coefficient of water
P_i partial pressure of species
P° ambient pressure
R universal gas constant (8.314 J $mol^{-1}\ K^{-1}$)
T cell operating temperature (K)
z number of released electrons

Greek symbols
α_α anode transfer coefficient
α_c cathode transfer coefficient
γ_a order of anode reaction
γ_c order of cathode reaction
ΔG° Gibbs free energy of ethanol formation (-1326.7 kJ mol^{-1}, exothermic reaction)
ΔH° ethanol higher heating value
ε^{d} void volume fraction of diffusion layer
ε^{c} void volume fraction of catalyst layer
ε^{c}_{m} volume fraction of membrane
η_a anode activation overpotential (V)
η_c cathode activation overpotential (V)
η_{ohmic} ohmic overpotential (V)
$\eta_{crossover}$ overpotential due to the ethanol crossover (V)
$\eta_{conc,an}$ anode concentration overpotential (V)
$\eta_{conc,cath}$ cathode concentration overpotential (V)
ρ_{H_2O} density of water (1.0 g cm^{-3})

cathode performance and consequently on the whole fuel cell operation. The model calculations consider mass transport in the porous diffusion media, as well as, mass transport and electrochemical reactions within the porous catalyst layers that contain fraction of an ion-conducting electrolyte material. Mass transport within the ion-conducting polymer electrolyte membrane (PEM) that is in part diffusive and in part caused by electro-osmosis is considered. The model is developed on the basis of an earlier DE-PEMFC work [36], and validated against literature experimental results [11,12].

Additional information included in the present work is: (a) the equations used for the mathematical modeling of the humidified oxygen transport and its reduction within the cathode side of the cell, (b) the direct correlation between the ethanol crossover rate and the parasitic current formation at the cathode side, (c) the investigation of the mixed overpotential, (d) the equations for the concentration polarization at both the anode and the cathode compartments of the cell and (e) the effect of the oxygen feed concentration on the cell performance.

2. Theory

The domain and the physico-electrochemical processes considered in the present investigation are schematically depicted in Fig. 1. The ethanol–water mixture is fed into the anode flow channel. As it can be seen, the diffusion and the catalyst layers are located next to the flow channels. The diffusion layer is made

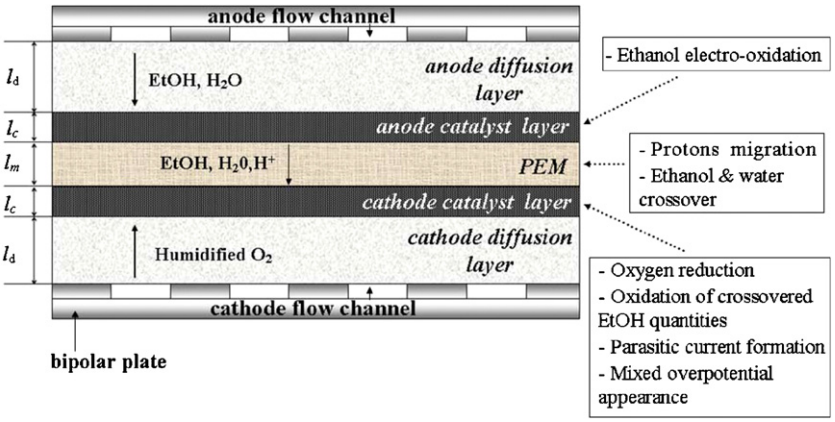

Fig. 1. Schematic of a single DE-PEMFC with the operational principles depicted.

by porous and electrically conductive material, through which, the electrons generated in the anode catalyst layer are transported to the current collector. The catalyst layer is the place where the ethanol electro-oxidation takes place, and in the ideal case of the complete electro-oxidation of a molecule of ethanol, 12 protons and 12 electrons would be released as follows:

$$\text{Anode}: \quad C_2H_5OH + 3H_2O \rightarrow 2CO_2 + 12H^+ + 12e^- \quad (1)$$

$$\text{Cathode}: \quad 12H^+ + 12e^- + 3O_2 \rightarrow 6H_2O \quad (2)$$

$$\text{Overall}: \quad C_2H_5OH + 3O_2 \rightarrow 2CO_2 + 3H_2O \quad (3)$$

However, in DEFCs below 100 °C the electro-oxidation of ethanol does not proceed all the way to carbon dioxide (CO_2), but rather to acetaldehyde (CH_3CHO), acetic acid (CH_3COOH), and CO_2 depending on the nature and structure of the catalyst used, the applied potential, and the temperature field established. Acetaldehyde was reported to be the main product of ethanol oxidation in early investigations [39].

At room or moderate temperatures, pure platinum, Pt, is not a very good anode catalyst for ethanol or methanol electro-oxidation as it is poisoned by strongly adsorbed intermediates. Adsorbed carbon monoxide, CO_{ads}, is a species always present in the anodic reaction mechanism leading to anode poisoning, thereby to considerable anodic overpotentials compared to the theoretical possible fuel cell voltages. In a study of oxidation of ethanol at a platinum electrode in perchloric acid solution via *in situ* IR reflection–absorption spectroscopy at constant potentials [40] only linearly adsorbed CO was detected as a surface species. At high ethanol concentrations this species was observed even at high anodic potentials where bulk ethanol oxidation takes place. In the same study acetaldehyde, carbon dioxide, and acetic acid were observed as bulk products. Making alloys of platinum with a second or third metal, among them ruthenium, Ru, is a convenient way to overcome poisoning due to electro-oxidation reaction intermediates, especially the adsorbed CO. Based on the bi-functional mechanism for electro-oxidation [41] Ru activates water molecules and provides preferential sites for $–OH_{ads}$ adsorption at lower than Pt potentials. Abundant $–OH_{ads}$ species are necessary to completely oxidize the poisoning intermediates to CO_2. It has been confirmed that the electrocatalytic activity of Pt for ethanol oxidation can be greatly enhanced by the addition of tin, (Sn) [2,11,42,43]. The nature and structure of the anode catalysts play a key role on adsorption and electro-oxidation of ethanol and other alcohols [44] whereas increasing the operation temperature range of PEMFCs directly fed with liquid ethanol can increase the rate of electro-oxidation reaction, thereby decreasing the anode overpotential. Pt-Ru catalysts show almost a comparable activity for ethanol and methanol electro-oxidation at 170 °C as reported in [45].

Taking into consideration the findings of the reaction products analysis and the released electrons over a Pt-Sn/C, Pt-Sn-Ru/C [16] and a Pt-Ru/C [46], the main products of the ethanol electro-oxidation are acetaldehyde, acetic acid and CO_2, whereas approximately 3–4 electrons are released [16,47–49]. The number of the released electrons is strongly dependent on the catalyst used for the ethanol electro-oxidation, the whole process of the catalyst preparation that affects its structural and electrochemical characteristics [2] and the cell operating temperature. Thus, in the present theoretical investigation it is considered that 4 electrons are released, as reported elsewhere as well [49]. The detailed reaction mechanism for the ethanol electrooxidation over Pt and Pt based binary electrocatalysts is thoroughly presented in the literature [1,9,47,49]. Protons and electrons are then transported to the cathode side of the cell but in different ways: electrons through an external circuit while protons via PEM. Protons and electrons are consumed at the cathode side by reacting with the humidified oxygen for water production. Apart from the protons transported through PEM, ethanol and water crossover to the cathode side as well. The presence of ethanol at the cathode catalyst hinders the oxygen reduction resulting in the formation of a mixed overpotential (ideal cathode overpotential due to oxygen reduction reaction (ORR) + overpotential due to ethanol crossover and subsequent ethanol electrocatalytic oxidation reaction (EOR)).

For the mathematical model development the following assumptions were made: (a) equations are defined in one direction; (b) the cell is operated under steady-state, isothermal conditions; (c) model considers neither a two-phase flow regime nor a phase change taking place during operation; (d) oxygen permeation through the PEM is negligible; and (e) from the crossovered quantity of ethanol, which is electro-oxidized over

the cathode catalyst, the number of the released electrons is the same as those released over the anode catalyst.

2.1. Model equations, anode compartment

The equations used for the mathematical model concerning the anode compartment of the cell have already been reported in detail elsewhere [36]. In the present investigation the mathematical model analysis is based on the assumption that ethanol is mainly electro-oxidized to acetic acid, acetaldehyde and CO_2. Based on the above discussion the main equations for both the anode and the cathode compartments are reported below.

In the catalyst layer the rate of the ethanol electro-oxidation can be described from the Butler–Volmer equation and in a simpler way by the Tafel approximation:

$$\frac{\mathrm{d}i}{\mathrm{d}z} = A_v i_{\mathrm{o,ref}} \left(\frac{C_{\mathrm{EtOH}}}{C^{\mathrm{ref}}_{\mathrm{EtOH}}} \right)^{\gamma} \exp\left(\frac{z_{\mathrm{a}} a_{\mathrm{a}} F \eta_{\mathrm{a}}}{RT} \right) \tag{4}$$

where i is the local protonic current density, $A_v i_{\mathrm{o,ref}}$, the anode reference exchange current density times area, γ, the order of reaction, z_{a} (=4e$^-$), is the number of the electrons released in the anode reaction, C_{EtOH}, the local ethanol concentration in the catalyst layer, a_{a}, the anode transfer coefficient, while η_{a} is the anode activation overpotential. The catalyst layer has a complex three-dimensional microstructure; therefore, to convert the electrocatalytic surface reaction rate (Butler–Volmer or Tafel equation) into a volumetric reaction rate, A_v, the specific reaction surface area (effective catalyst surface area per unit geometric volume of the catalyst layer) is employed incorporating the noble metal loading into the model as well. The specific reaction surface area, A_v, is given by $A_v = m_{\mathrm{cat}} A_{\mathrm{s}} / l^{\mathrm{c}}_{\mathrm{an,\,cath}}$ where m_{cat} is the catalyst mass loading per unit area of the electrode, A_{s} is the catalyst surface area per unit mass of the catalyst, and $l^{\mathrm{c}}_{\mathrm{an,\,cath}}$ is the anode/cathode catalyst layer thickness as in the work [50]. The catalyst surface area may vary considerably for different types of supported catalysts and platinum black. In the present investigation, the specific reaction surface area A_v is calculated according to the data found for a 20% Pt/C and the value of the exchange current density is calculated from the experimental data of the cited work [12]. Furthermore, the value of the anode transfer coefficient was extracted from the same experimental data—PtRu/C anode catalyst (1.0 mg cm^{-2} Pt) assuming for each ethanol molecule the release of 4 e$^-$. From the Tafel slope, the anodic transfer coefficient, α_{a}, is calculated ($\alpha_{\mathrm{a}} = RT/z_{\mathrm{a}} f_{\mathrm{a}} F$) where f_{a} is the anodic Tafel slope with the natural base e in contrast to the decade Tafel slope $b = 2.3 f_{\mathrm{a}}$. It is found to be 0.089, close to the value reported for the ethanol electro-oxidation over Palladium (Pd) electrodeposited on Titanium (Ti) ($\alpha_{\mathrm{a}} = 0.1$) [51]. As it was previously mentioned, the electrochemical characteristics of a catalyst are directly correlated with the metal loading, the mean particle size of the catalyst, the lattice parameter, the thermal treatment of the catalyst and generally the whole process of preparation for the catalyst [2].

The dominant mechanisms concerning the ethanol and water flux through the anode catalyst layer are the diffusion and the electro osmosis. From the ethanol electrooxidation mechanism [48] when the main product of the ethanol oxidation is acetic acid with four electrons released, the stoichiometric ethanol to water ratio is 1:1. Consequently, the fluxes of the two species can be described as follows:

$$N_{\mathrm{EtOH}} = -D^{\mathrm{c,eff}}_{\mathrm{EtOH}} \frac{\mathrm{d}C_{\mathrm{EtOH}}}{\mathrm{d}z} + \frac{C_{\mathrm{EtOH}}}{C_{\mathrm{H_2O}} + C_{\mathrm{EtOH}}} N_{\mathrm{H_2O}} \tag{5}$$

$$N_{\mathrm{H_2O}} = \frac{I - i}{4F} + N^{\mathrm{m}}_{\mathrm{H_2O}} \tag{6}$$

$D^{\mathrm{c,eff}}_{\mathrm{EtOH}}$ stands for the effective diffusion coefficient of ethanol in the catalyst layer, $N_{\mathrm{H_2O}}$ for the local water flux, I for the operating cell current density, and i, for the protonic current density.

Water and ethanol transport through the PEM is the result of the following three phenomena: electro-osmosis, diffusion and hydraulic permeation. Based on the assumption that, at both the anode and the cathode side the pressure is equal, it can be deduced that only the first two phenomena take effect:

$$N^{\mathrm{m}}_{\mathrm{H_2O}} = N_{\mathrm{electrdrag}} + N_{\mathrm{diff}} \tag{7}$$

$N_{\mathrm{electrdrag}}$ denotes the water flux caused by the electro-osmotic drag, which at a constant cell temperature is linearly depended on the cell current density I, and it can be expressed as follows:

$$N_{\mathrm{electrdrag}} = n_{\mathrm{H_2O/drag}} \frac{I}{F} \tag{8}$$

where $n_{\mathrm{H_2O/drag}}$, is the electro-osmotic drag coefficient of water. N_{diff} is deduced from the water concentration gradient through PEM and expressed by:

$$N_{\mathrm{diff}} = D^{\mathrm{m}}_{\mathrm{H_2O}} \frac{C^{\mathrm{an}}_{\mathrm{H_2O}} - C^{\mathrm{cath}}_{\mathrm{H_2O}}}{l_{\mathrm{m}}} \tag{9}$$

$D^{\mathrm{m}}_{\mathrm{H_2O}}$ represents the diffusion coefficient of water in PEM, l_{m} the PEM's thickness and $C^{\mathrm{an}}_{\mathrm{H_2O}}$, $C^{\mathrm{cath}}_{\mathrm{H_2O}}$ the water concentration at the anode and the cathode side respectively. For the sake of simplicity, based on the assumption that both anode and cathode are fully hydrated, water transport through the membrane can be reduced into:

$$N^{\mathrm{m}}_{\mathrm{H_2O}} \cong n_{\mathrm{H_2O/drag}} \frac{I}{F} \tag{10}$$

eliminating the water diffusion transport. Thus, the ethanol crossover through PEM can be expressed from Eq. (11) [36]:

$$N^{\mathrm{m}}_{\mathrm{EtOH}} = \frac{C^{\mathrm{an}}_{\mathrm{EtOH}} e^{v^{\mathrm{m}}/k^{\mathrm{m}}} - C^{\mathrm{cath}}_{\mathrm{EtOH}}}{e^{v^{\mathrm{m}}/k^{\mathrm{m}}} - 1} v^{\mathrm{m}} \tag{11}$$

where $k^{\mathrm{m}} = D^{\mathrm{m}}_{\mathrm{EtOH}} / l_{\mathrm{m}}$, is the mass transfer coefficient of ethanol within PEM, $C^{\mathrm{an}}_{\mathrm{EtOH}}$ and $C^{\mathrm{cath}}_{\mathrm{EtOH}}$ ethanol concentration at the anode and cathode sides of PEM respectively and $v^{\mathrm{m}} = \mathrm{M_{H_2O}} \mathrm{N^m_{H_2O}} / \rho_{\mathrm{H_2O}}$ the superficial velocity of water through PEM. The presence of ethanol at the cathode side is due to the ethanol crossover from the anode side. Based on the assumption that the crossovered ethanol concentration is much less compared to the anode concentration and it is oxidized over the cathode catalyst

[22,26,36], leading to the formation of mixed overpotential, Eq. (11) is reduced into Eq. (12):

$$N^{m}_{EtOH} = \frac{C^{an}_{EtOH} e^{v^m/k^m}}{e^{v^m/k^m} - 1} v^m \quad (12)$$

2.2. Model equations, cathode compartment

In a similar way the description of the humidified oxygen mass transport at the cathode compartment can be performed. Eq. (13) is used to describe the humidified oxygen transport from the cathode flow channel to the cathode diffusion layer:

$$N^{d}_{O_2} = k_c(C_{F,O_2} - C_{s,O_2}) \quad (13)$$

where $N^{d}_{O_2}$ stands for the oxygen flux through the diffusion layer, C_{F,O_2} for the oxygen feed concentration, C_{s,O_2} for the ethanol concentration at the surface of the diffusion layer, and k_c for the mass transfer coefficient.

The flux of water though the cathode diffusion layer can be described by Eq. (14):

$$N^{d,cath}_{H_2O} = \frac{I}{4F} + N^{m}_{H_2O} \quad (14)$$

Here $N^{d,cath}_{H_2O}$ is the flux of water through the cathode diffusion layer. The oxygen flux at the diffusion layer can be described from the following equation:

$$N^{d}_{O_2} = -D^{d,eff}_{O_2} \frac{dC_{O_2}}{dz} + \frac{M_{H_2O} C_{O_2}}{\rho_{H_2O}} N^{d,cath}_{H_2O} \quad (15)$$

Here $D^{d,eff}_{O_2}$ stands for the effective diffusion coefficient of oxygen in the diffusion layer, and $N^{d,cath}_{H_2O}$ the total flux of both water and oxygen. Assuming that $D^{d,eff}_{O_2}$ and ρ_{H_2O} are constant, the solution of the equation, within the intervals of the cathode diffusion layer, is the following:

$$N^{d}_{O_2} = \frac{C_{F,O_2} e^{v^d/k^d} - C^{o}_{O_2}}{e^{v^d/k^d}((v^d/k^d) + 1) - 1} v^d \quad (16)$$

where $k^d = D^{d,eff}_{O_2}/l^{d}_{cath}$ is the mass transfer coefficient of oxygen within the diffusion layer, and $v^d = M_{H_2O} N^{d}_{H_2O}/\rho_{H_2O}$ the superficial velocity of water through the cathode diffusion layer.

In the cathode catalyst layer the oxygen transport is similar to that of the cathode diffusion layer, so the local oxygen flux can be expressed in a similar way:

$$N^{c}_{O_2} = -D^{c,eff}_{O_2} \frac{dC_{O_2}}{dz} + \frac{M_{H_2O} C_{O_2}}{\rho_{H_2O}} N^{c,cath}_{H_2O} \quad (17)$$

Here $D^{c,eff}_{O_2}$ denotes the effective diffusion coefficient of oxygen in the diffusion layer, and $N^{c,cath}_{H_2O}$ the water flux through the cathode catalyst layer.

The flux of oxygen in the cathode catalyst layer decreases due to its reduction over the catalytic sites; hence the material balance for oxygen within the intervals of the cathode catalyst layer is as follows [52]:

$$\frac{dC_{O_2}}{dz} = -\left(\frac{(I + I_p) - i}{4F D^{c,eff}_{O_2}}\right) \quad (18)$$

Tafel kinetics with first order oxygen concentration dependence is employed to describe the rate of ORR at the cathode catalyst layer, where the Tafel slope (calculated as follows: $2.303RT/z_c a_c F$) for ORR at 298 K falls anywhere between 60 mV dec^{-1} and 120 mV dec^{-1} (i.e. $z_c a_c = 0.5$–1.0) in the absence of simultaneous alcohol oxidation [53,54]. However, in Direct Alcohol Fuel Cells (DAFCs), ORR takes place simultaneously with oxidation of crossover alcohol, and as a result the Tafel slope for a DAFC should become greater than that for a hydrogen/air PEMFC. This behavior has been observed and reported for ORR with simultaneous methanol oxidation reaction (MOR) on Pt under acidic media in [55–57].

The Tafel equation is written for the rate-determining step and the number of electrons transferred is 1 [54,55,57], and the following expression is used [58]:

$$I + I_p = A_v i^{O_2}_{o,ref} \frac{C_{O_2}}{C^{ref}_{O_2}} \exp(z_c a_c \eta_c F/RT) \quad (19)$$

Here I_p is the parasitic current originated from the crossovered ethanol quantities electro-oxidation at the cathode catalyst layer. I_p has a similar expression as it has been reported elsewhere for a direct methanol fuel cell [28,58]:

$$I_p = z_a F N^{m}_{EtOH} \quad (20)$$

Moreover, the values for the cathode transfer coefficient a_c and the cathode reference exchange current density times area, reported in Table 1, are chosen as follows: The value for the exchange current density was extracted from the literature work [57]. The value for the cathode reference exchange current density times area, $A_v i^{O_2}_{o,ref}$ was calculated in a similar way for a 20% Pt/C with that concerning the anode reference exchange current density times area. Furthermore, the value for the cathode transfer coefficient, α_c, was chosen equal to 1.0, resulted from a Tafel slope of ~59 mV dec^{-1} at 298 K. This value is consistent with what has been recently reported in [55]. It should be pointed out that in the case of DAFCs, the alcohol crossovered from the anode to the cathode compartment seriously affects the oxygen reduction over the cathode catalyst. Similarly to what it was found in the case of mixed methanol oxidation and oxygen reduction over a carbon supported Pt catalyst [57], in DEFCs the crossovered ethanol oxidation current should be slightly affected by the presence of oxygen, while the oxygen reduction current is drastically suppressed by the surface intermediates originated from the oxidation process. Furthermore, as in indicated in [56] for a DMFC, the poisoning effect of the presence of methanol on oxygen reduction reaction was confirmed to be significant, especially when the cell operates at higher methanol concentrations.

Table 1
Base-case parameter values

Temperature (K)	363
Diffusion coefficient of ethanol to water, D_{EtOH-H_2O} ($cm^2\,s^{-1}$)	0.1548 [67]
Effective diffusion coefficient of ethanol in diffusion layer, $D^{d,eff}_{EtOH}$ ($cm^2\,s^{-1}$)	3.916×10^{-2}
Effective diffusion coefficient of ethanol in catalyst layer, $D^{c,eff}_{EtOH}$ ($cm^2\,s^{-1}$)	8.109×10^{-3}
Diffusion coefficient of oxygen in water, $D_{O_2-H_2O}$ ($cm^2\,s^{-1}$)	0.338 [67–69]
Effective diffusion coefficient of oxygen in diffusion layer $D^{d,eff}_{O_2}$ ($cm^2\,s^{-1}$)	8.55×10^{-2}
Effective diffusion coefficient of oxygen in catalyst layer $D^{c,eff}_{O_2}$ ($cm^2\,s^{-1}$)	1.77×10^{-2}
Effective diffusion coefficient of ethanol in membrane, $D^{m,eff}_{EtOH}$ ($cm^2\,s^{-1}$)	1.73×10^{-6} [12,70]
Anode diffusion layer thickness, l^d_{an} (μm)	140 [26]
Cathode diffusion layer thickness, l^d_{cath} (μm)	140 same as anode
Anode catalyst layer thickness, l^c_{an} (μm)	10 [22,36]
Cathode catalyst layer thickness, l^c_{cath} (μm)	10 same as anode
Nafion 115 membrane thickness, l_m (μm)	127 [70]
Reference ethanol molar concentration, C^{ref}_{EtOH} ($mol\,L^{-1}$)	0.5 [36]
Reference oxygen molar concentration, $C^{ref}_{O_2}$ @363 K and 1 atm, ($mol\,cm^{-3}$)	0.3289×10^{-6} [57]
Protonic conductivity of ionomer, K_m ($S\,cm^{-1}$)	0.1416 [27]
Anode transfer coefficient, α_a	0.089 [12]
Cathode transfer coefficient, α_c	1.0 [35,55]
Order of reaction (anode), γ_a	0.25 [36]
Order of reaction (cathode), γ_c	1 [63]
Anode specific reaction surface area, A_v (m^{-1}) (20% Pt/C) 1.33 mg	1.489×10^8 [11,50]
Anode specific reaction surface area, A_v (m^{-1}) (20% Pt/C) 1.00 mg	$1.12\ 10^8$
Cathode specific reaction surface area, A_v (m^{-1}) (20% Pt/C) 1.00 mg	$1.12\ 10^8$
Anode reference exchange current density times area, $A_v i_{o,ref}$ ($A\,cm^{-3}$)	0.1172 [12,50]
Cathode reference exchange current density times area, $A_v i^{O_2}_{o,ref}$ ($A\,cm^{-3}$)	4.82×10^{-2} [50,57]
Electronic conductivity of solid phase (PtRu/C), K_s ($S\,cm^{-1}$)	8.13×10^{-6} [20]
Feed oxygen molar concentration, C_{F,O_2} ($mol\,cm^{-3}$)	4.2×10^{-5}
Void volume fraction of anode diffusion layer, ε^d	0.4 [28]
Void volume fraction of cathode diffusion layer, ε^d	Same as anode
Void volume fraction of anode catalyst layers, ε^c	0.35
Void volume fraction of cathode catalyst layers, ε^c	Same as anode
Volume fraction of ionomer phase in catalyst layer, ε^m	0.14
Electrosmotic drag coefficient, $n_{H_2O/drag}$	3.16 [71,72]

2.3. Equations used for the calculation of the total cell potential

The total cell potential is obtained by the following equation:

$$V_{cell} = E^{Nernst} - \eta_\alpha - \eta_c - \eta_{ohmic} - \eta_{crossover} - \eta_{conc,an} - \eta_{conc,cath} \quad (21)$$

Here V_{cell} denotes the fuel cell potential, E^{Nernst} is the Nernst potential of the fuel cell at the operating temperature, η_α the anode activation overpotential, η_c the cathode activation overpotential, η_{ohmic} the ohmic overpotential (loss in the membrane and losses between the contacts), $\eta_{conc,an}$ the anode concentration overpotential and $\eta_{conc,cath}$ the cathode concentration overpotential.

All the thermodynamic calculations are presented in detail in Appendix A.1.

The ohmic overpotential is the combined result of the losses during the proton transport through the membrane (η_{membr}) and the losses between the contacts of the fuel cell components ($\eta_{contact}$).

$$\eta_{ohmic} = \eta_{membr} + \eta_{contact} \quad (22)$$

$$\eta_{membr} = \frac{l_m}{K^{eff}_m} I \quad (23)$$

$$\eta_{contact} = \frac{(l_m + l^c_{an} + l^c_{cath} + l^d_{an} + l^d_{cath})}{K^{eff}_s} I \quad (24)$$

The anode and cathode concentration overpotentials developed over the anode and the cathode catalyst respectively could be expressed as follows [59]:

$$\eta_{conc,an} = \frac{RT}{zF} \ln\left(\frac{I_{lim,an}}{I_{lim,an} - (I + I_p)}\right) \quad (25)$$

$$\eta_{conc,cath} = \frac{RT}{zF} \ln\left(\frac{I_{lim,cath}}{I_{lim,cath} - (I + I_p)}\right) \quad (26)$$

Here $I_{lim,an}$ and $I_{lim,cath}$ are the limiting current densities at the anode and the cathode compartment respectively, resulting from the ethanol and oxygen respectively mass transport limitations. The theoretical limiting current could be expressed as follows [28,59]:

$$I_{lim,i} = z_{a/c} F D_i \frac{C_{i,bulk}}{l_d} \quad (27)$$

$I_{\lim,i}$ is the limiting current of each species (ethanol and oxygen), D_i is the species effective diffusivity, l_d the anode and cathode compartments' thickness and $z_{a/c}$ the released electrons.

It should be noted that all the effective transport coefficients (diffusivities, protonic and electronic conductivity) were calculated through the Bruggeman's correction for porous media. As an example, the ethanol's effective diffusivity is given as:

$$D_{\mathrm{EtOH}}^{\mathrm{d,eff}} = (\varepsilon^{\mathrm{d}})^{3/2} D_{\mathrm{EtOH-H_2O}} \quad (28)$$

Moreover, it should be noticed that the oxygen flows through an external saturator operating at ambient temperature and then reaches the cathode flow channel. From thermodynamic tables [60] the following parameters are obtained. At $T = 303$ K, and pressure 1 bar, the saturation pressure of water is 4.24 kPa. Considering the mixture as ideal [61], from mathematical calculations the pure oxygen feed concentration is approximately 4.2×10^{-5} mol cm^{-3} and this value is used as the base case value for the oxygen feed molar concentration ($C_{\mathrm{F,O_2}}$).

The values of the parameters used in the present model are presented in Table 1. Most of them are from the literature and the rest are design parameters.

3. Results and discussion

A fourth order Runge–Kutta method [62] implemented in an in-house self-written FORTRAN code is employed for the numerical solution of the system of the governing differential equations.

3.1. Model validation

For the validation of the present model the simulation results are compared with the experimental data taken from two different literature works [11,12] In Fig. 2a a comparison between the experimental curves from two different DE-PEMFCs operation and the mathematical model predictions is presented. The experimental data (#1) concern the DE-PEMFC operation when an in-house PtRu/C (1.0 mg cm^{-2} Pt) anode catalyst and a commercial 20% Pt/C (1.0 mg cm^{-2} Pt) cathode catalyst (Johnson Matthey Corp.) were used [12]. The second experimental data (#2) were taken from a DE-PEMFC operation when a PtRu/C (1.33 mg cm^{-2} Pt) anode catalyst and a commercial Pt/C (1.0 mg cm^{-2} Pt) cathode catalyst (Johnson Matthey Corp.) were used. Nafion®-115 membrane was used as solid electrolyte, which was pre-treated with diluted H_2O_2 solution and H_2SO_4 solution successively. The cell with an active area of 9 cm^{-2} was fed with an aqueous ethanol solution of 1.0 mol L^{-1} and the fuel flow rate was 1.0 mL min^{-1}. On the cathode side the oxygen was fed with a total flow rate of 120 mL min^{-1} and pressure of 0.2 MPa [11].

As it can be seen from Fig. 2a, a relatively good agreement was found. The difference in Pt loading between the two experiments was taken into account in the mathematical model through the value of $A_v i_{\mathrm{o,ref}}$ (the specific reaction surface area per unit mass of the catalyst is multiplied with the exchange current density calculated from the experimental results [12]).

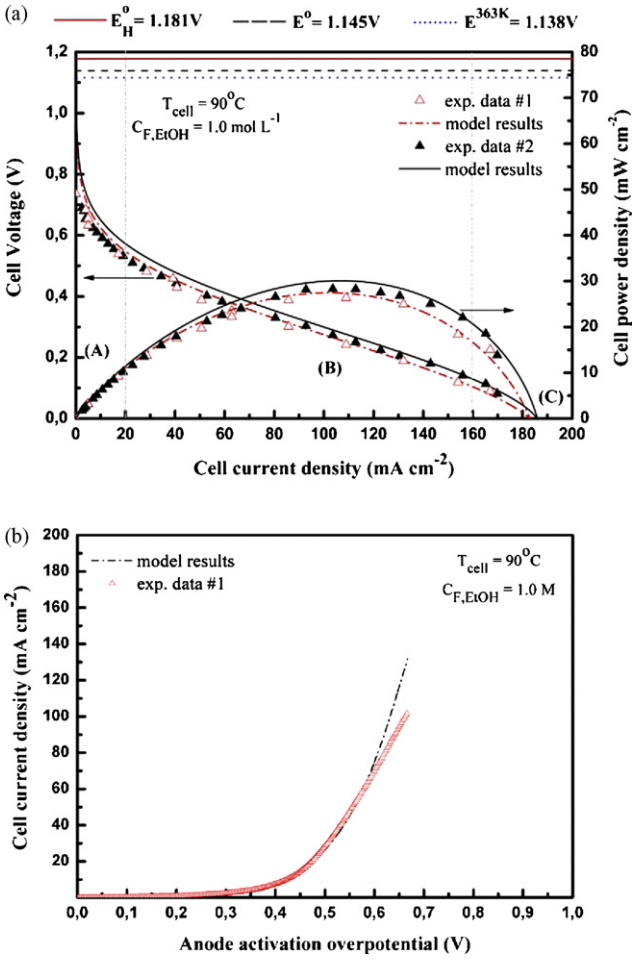

Fig. 2. (a) Validation of the predicted *I–V* curves against experimental data reported in (#1)[12], (#2) [11]. (#1): DEFC performance @ 90 °C, PtRu/C anode catalyst with 1.0 mg cm^{-2} Pt; (#2) DEFC performance @ 90 °C, PtRu/C anode catalyst with 1.33 mg cm^{-2} Pt. In both cases Nafion®-115 membrane and Pt/C cathode catalysts were used. E_{H}° thermo-neutral potential corresponding to HHV of ethanol, E° theoretical potential, $E^{363\,\mathrm{K}}$ Nernst potential of the DE-PEMFC @ $T = 363$ K. (b) Validation of the anode polarization curve against experimental data reported in (#1) [12].

The thermo-neutral potential E_{H}°, the standard reversible potential E° @ 298 K and the Nernst potential @ 363 K, $E^{\mathrm{Nernst,\,363\,K}}$ of a DEFC are also given in the figure. The thermodynamic calculations are reported in detail in Appendix A. As it can be seen, there are voltage losses between the thermo-neutral potential and the theoretical potential, which are attributed to the entropy term ($T\Delta S/zF$). The Nernst potential at 363 K is lower than the theoretical potential (@ $T = 298$ K) due to the increased operating temperature value. The real operation of the cell is the one denoted by the experimental data. Three distinct regions are discernible (A, B, C). In the activation overpotential region (region A) there is good agreement between the experimental data and the model predictions. At B and especially C regions known as region of ohmic polarization and region of concentration polarization respectively, the difference between the experiments and the model predictions is lower and slightly higher respectively. It is worth noticing that a 1-D, single phase, isothermal mathematical model affects the accuracy of the model results especially in the concentration polarization region. More

specifically, predictions concerning the mass fluxes distribution of both ethanol and water in the anode and the cathode compartments and thus electrical performance *V–I*, *P–I* curves are overestimated in comparison to a multi-dimensional mathematical model based analysis [37]. With the addition of two phase flow with capillary effects in both anode and cathode backings, model predictions are even closer to the experimental data, as it was shown for a DMFC model elsewhere [30,34]. Although heat transfer and liquid–gas two-phase flow effects are expected to play an important role in direct alcohol fuel cell operation and performance, the present single-phase implementation leads to a computationally simplified formulation of the situation with a reasonable degree of accuracy of the predicted DEFC performance. More precisely, the error estimation between the model predictions for the cell voltage and the experimental data is reported in Table A1 (cf. Appendix A.2).

Moreover, Fig. 2b compares the calculated anode overpotential using the present model with the experimental data of (#1).

3.2. Anode and cathode activation overpotentials—mixed overpotential

Fig. 3a and b depicts the anode and the cathode activation overpotentials respectively as a function of the cell current density. The ethanol feed concentration is 1.0 mol L^{-1}. Both activation overpotentials increase as the cell's charge increases. Additionally, from Fig. 3, in a DE-PEMFC, the anode activation overpotential is almost 5.8 times higher than the cathode one @ 40 mA cm^{-2}, reaching approximately a 6.5 times higher value close to the maximum current density. This is explained from the fact that the ethanol electro-oxidation rate, taking place at the anode, is much slower than the oxygen reduction rate at the cathode side of the cell [1]. This is the reason why so many experimental works have been recently devoted to the development of novel binary–ternary anode electrocatalysts that would exhibit higher electrocatalytic activity for the fuel (ethanol) oxidation. Furthermore, it is worth noticing that between the current density and the anode overpotential an exponential dependence is observed. As it can be also seen in Fig. 3a the anode activation overpotential is rapidly increased as the current density ranges from almost 0 mA cm^{-2} up to 60 mA cm^{-2}. After this value, the overpotential increment is smoother. Finally, close to the limiting current density value, there is a sharp increment of the anode activation overpotential due to the anode mass transfer limitations. This behavior could be explained from the fact that at low overpotential values, the electro-oxidation of ethanol is controlled by the slow kinetics, while at higher proceeds more easily [36].

In Fig. 3b, the mixed overpotential is analyzed by examining the cathode activation overpotential when the parasitic current is enabled and disabled. As it was mentioned previously, the parasitic current is the result of the crossovered ethanol oxidation at the cathode catalyst that hinders the oxygen reduction over the cathode catalyst. More precisely, the ethanol crossovered amounts are oxidized over the same catalytic active sites, where the oxygen reduction would take place if oxygen were the sole

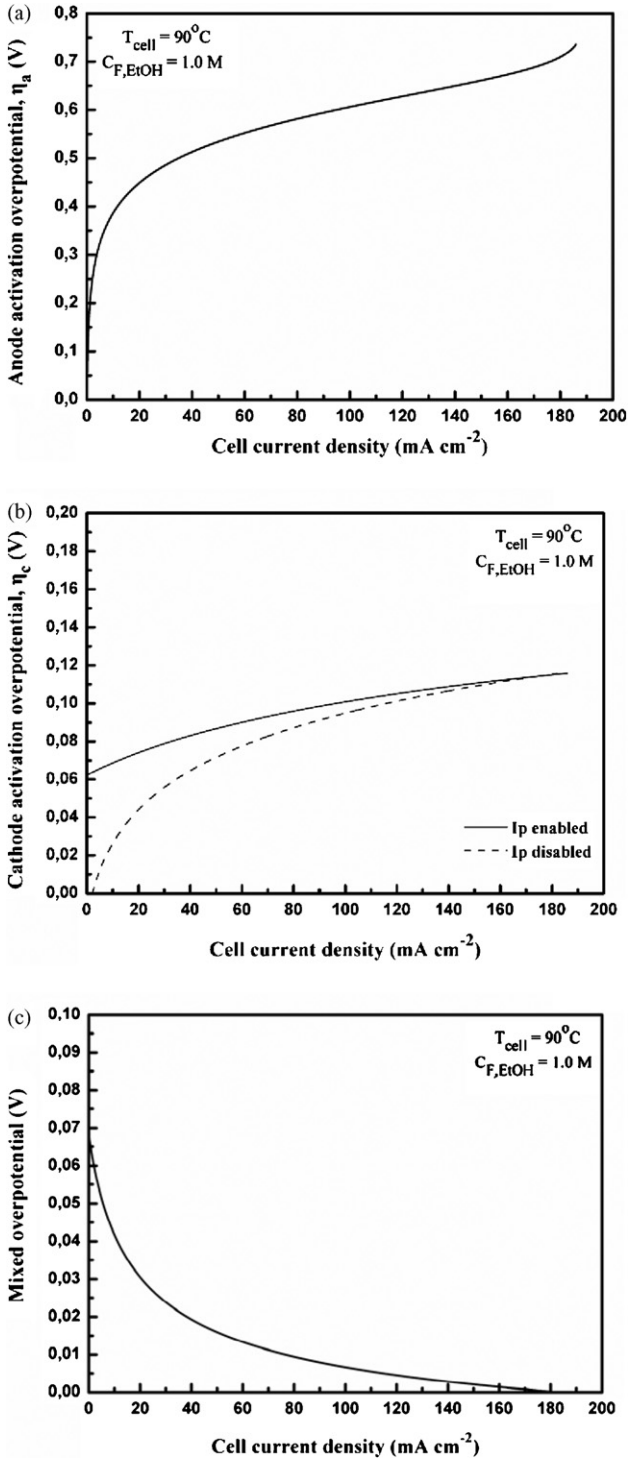

Fig. 3. (a) Anode activation overpotential vs. cell current density. (b) Cathode activation overpotential vs. cell current density: I_p enabled–I_p disabled. (c) Mixed overpotential due to crossovered ethanol as a function of the operating current density.

species present within the cathode catalyst layer, or they react directly with the oxygen molecules. Consequently, the oxygen reduction is hindered resulting to this mixed overpotential formation. In the present study, in the case of the disabled parasitic current, ethanol still crossovers the membrane, as in the case of the enabled parasitic current, however it is assumed that it is not

oxidized at all over the cathode catalyst. For the given operating parameters, the difference between the two cases decreases while the current density value increases. This is explained by the fact that the mixed overpotential is attributed to the parasitic current, which has direct relationship with the ethanol crossover rate. A similar observation appears in the literature concerning the direct methanol fuel cell operation [21,35].

The overpotential due to ethanol crossover, i.e. the difference between the cathode overpotential when ethanol electro-oxidation reaction taking place over the cathode catalyst layer and the case of no ethanol electro-oxidation reaction over the cathode catalyst layer as a function of current density is shown in Fig. 3c. It can be seen that ethanol crossover results in a substantially larger overpotential when the DEFC is at open circuit. However, even very low current density values (up to 40 mA cm^{-2}) can cause the crossover overpotential to fall sharply. It then decreases smoothly with increasing current density (>40 mA cm^{-2}), reaching the value of 0.001 mV at maximum current density. This is a consequence of the logarithmic nature of the overpotential/current density relation. Further explanation for the observed behavior is given below, where a direct correlation between the operating current density and the parasitic current is presented.

3.3. Ethanol crossover rate—parasitic current

Fig. 4 illustrates the effect of the cell operating current density on ethanol crossover rate and the parasitic current formation at the cathode side of the cell. The feed concentration at the anode side of the cell is 1.0 M. The ethanol crossover rate has its maximum value when the cell operates at open circuit voltage conditions. Furthermore, as the cell current density increases, the ethanol crossover rate is reduced, since more ethanol molecules are electro-oxidized at the anode compartment for electricity production. Thus, the concentration difference between the two sides of the cell is decreased, leading to less ethanol crossover rate. In addition, as the operating cell current density reaches its limiting value (limiting current) almost no ethanol concentration is available at the anode catalyst layer, due to mass transport limitations, resulting in the ethanol crossover rate decrement [28,35,36]. In the present work, the ethanol that reaches the cathode catalyst layer is oxidized resulting to the I_p formation. As it was previously discussed in the theory section, there is direct correlation between ethanol crossover rate and parasitic current. The effect of the cell operating current on the parasitic current formation is depicted in the same figure. The maximum I_p appears at the open circuit voltage where the ethanol crossover rate has its maximum value. Furthermore, I_p is reduced as the cell current density increases and is almost depleted when the ethanol crossover rate becomes very small. Finally, from this figure one can clearly understand the observed behavior between the cathode activation overpotentials (when the I_p is enabled and disabled) presented previously at Fig. 3b and c.

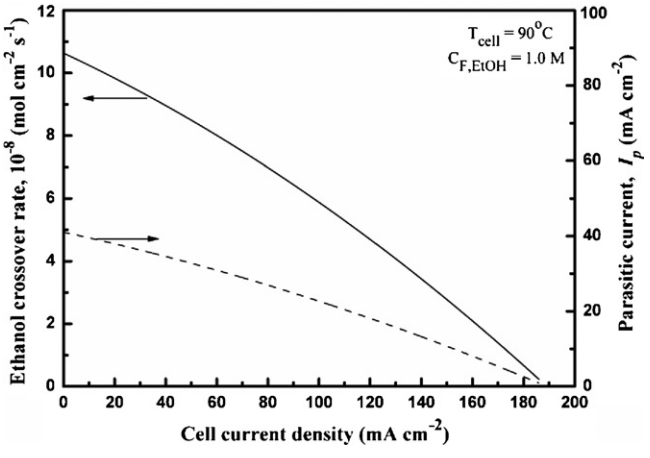

Fig. 4. Ethanol crossover rate and parasitic current formation vs. cell current density.

3.4. Ethanol–oxygen concentration profiles

The predicted variations of ethanol and oxygen concentrations, as a percentage of the feed concentration, within the anode and the cathode catalyst layers respectively, when the cell is operated at three different current density values are presented at Fig. 5a and b. It is observed that as ethanol passes through the anode catalyst layer, the predicted ethanol concentration through the catalyst is decreased. This is attributed to the fact that a thicker catalyst means more active sites, consequently more molecules could participate in the electrochemical reaction. Moreover, as the operating current density increases, the ethanol concentration reaching the catalyst layer is reduced. This is attributed to the fact that higher current density values lead to higher ethanol quantities that have to be consumed during the reaction. A similar behavior is predicted for the oxygen concentration profile through the cathode catalyst layer. As it can be distinguished from the oxygen concentration profiles, the oxygen reaching the cathode catalyst layer is less affected than the ethanol concentration profiles from the operating current density. A possible explanation is that the oxygen/water diffusivity is higher than the ethanol/water one, and consequently, their effective diffusivities within the porous catalyst layers have the same tendency. In the present investigation the oxygen concentration profiles slightly differ from other results presented elsewhere, concerning lower operating temperatures [28,63]. This is explained by the fact that the oxygen–water binary diffusivity value at the operating temperature (363 K) is much higher than the one at lower temperatures (i.e. 333 K). Thus, oxygen transport through the cathode catalyst layer is strongly governed by Fick's diffusion, when the cell is operated under the base case parameters' values. Fig. 5c depicts the spatial variation in reaction rate, di/dz, throughout the anode catalyst layer, for three operating current density values. In almost all cases, the reaction rate is little higher in the front part (z = 1) than in the back one (z = 0). Moreover, it was found that the reaction rate increases as the operating current increases. These findings could be explained by the fact that higher current densities lead to higher reaction rates for the cell to compensate the current density requirements. A similar observation concerning the reaction rate in a direct methanol PEM fuel cell was found elsewhere [22].

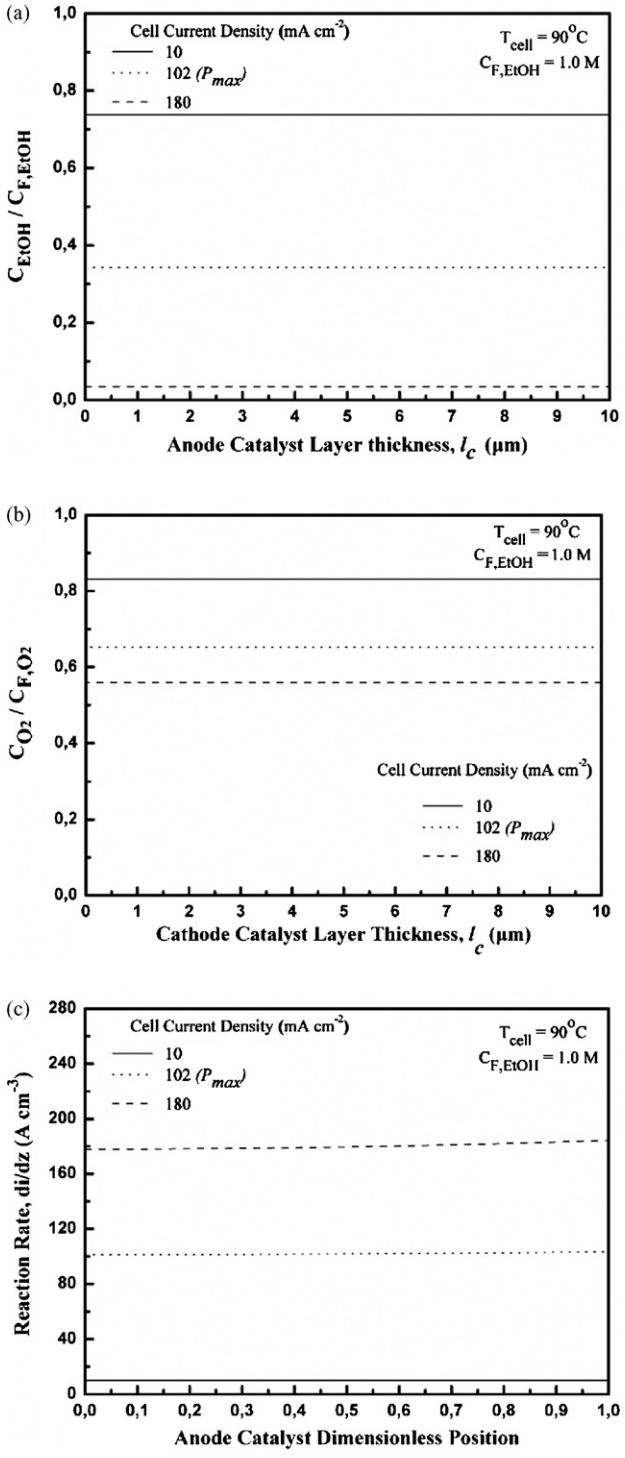

Fig. 5. (a) Predicted variation of ethanol concentration within the anode catalyst layer, (b) predicted variation of oxygen concentration within the cathode catalyst layer, (c) spatial variation of the reaction rate throughout the anode catalyst layer. Fuel cell is operated at three different current density values.

3.5. Anode and cathode concentration overpotentials in a DE-PEMFC—irreversibility ratio

The total concentration overpotential of a PEM fuel cell is the resultant effect of the anode and the cathode concentration overpotentials. One of the major problems that the hydrogen PEM fuel cells have to overcome is the mass transfer limitation concerning oxygen diffusivity at the cathode side of the cell. However, oxygen diffusivity seems not to be the major problem in a DE-PEMFC. As it can be distinguished from Fig. 6, during the DE-PEMFC operation the concentration overpotential of the anode side is much greater than the cathode side one. This is expected because the ethanol diffusivity through the anode compartment is much lower than oxygen's at the cathode side. Moreover, the released products of the ethanol electrooxidation at the anode side of the cell hinder more the ethanol diffusivity. Furthermore, the onset values for the anode and the cathode concentration overpotential are greater than zero and this is attributed to the presence of I_p that has its maximum value when the operating cell current density is zero. A closer look of Eqs. (25) and (26) justifies the above findings.

In Fig. 7a, the fractions of activation, ohmic and concentration overpotentials (irreversibilities) to the total overpotential, (named as irreversibility ratio) are plotted versus the cell operating current density. According to the model results, the activation polarization constitutes nearly 90% of the total overpotential occurring during the operation of the DE-PEMFC at low current density values. The concentration polarization has rising significance at higher current densities, especially at values close to the limiting current. The ohmic overpotential has minor contribution to the total overpotentials at low current densities however it increases at larger current densities. It should be noted that ohmic losses is the combined effect of the resistance to ion flow through the electrolyte and the electrical resistance during electron's flow at the electrodes. Lower resistances and ohmic losses can be obtained when electrodes with higher electrical conductivities are used. In the same direction, the electrolyte thickness and the protonic conductivity of the ionomer could reduce this irreversibility. However, this is particularly difficult, as the electrolyte needs to be thick enough for structural support of the electrodes. To conclude, a similar behavior concerning the entropy production in hydrogen PEM fuel cell appears in the literature [64]. In Table 2 each kind of the overpotentials

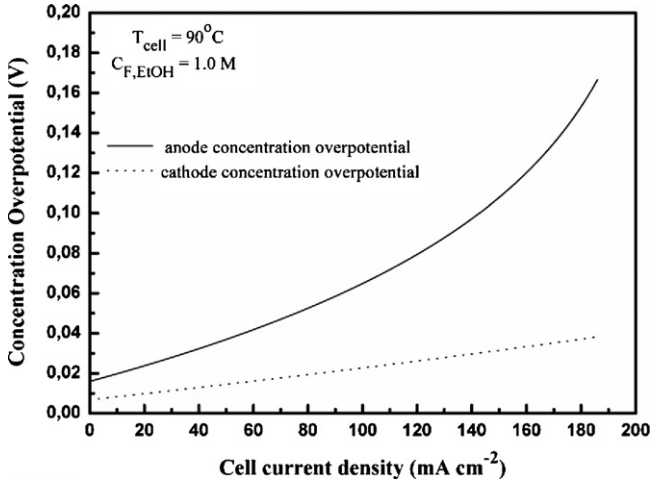

Fig. 6. Anode and cathode concentration overpotentials vs. operating cell current density.

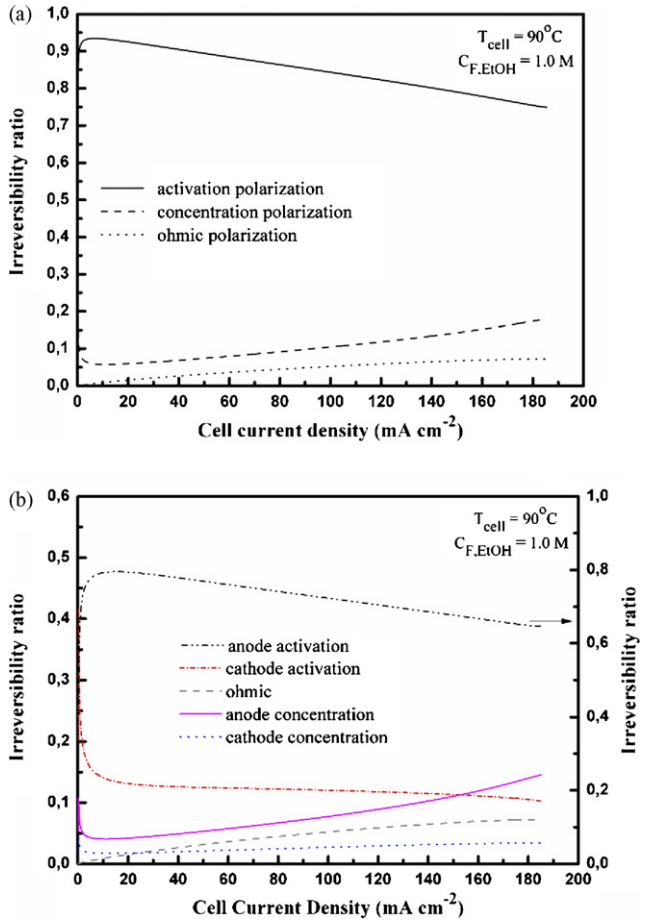

Fig. 7. (a) Direct Ethanol PEM Fuel Cell irreversibility ratio and (b) detailed representation of each irreversibility as a function of the operating current density.

as a percentage of the total overpotential occurring during the fuel cell operation at a wide range of current density values are presented. The exact percentage values are indicative of the above-mentioned discussion.

In Fig. 7b, a more detailed presentation of the irreversibilities is depicted. It is concluded that the anode activation polarization constitutes almost 70% of the total overpotentials occurring during the DE-PEMFC operation (right axis). This is attributed to the slow kinetics of the ethanol electro-oxidation over the anode catalyst layer. This finding explains why the recent years there is a huge number of experimental works dealing with the development of more active catalysts for the ethanol electro-oxidation [2,46]. Finally, the irreversibilities due to the oxygen reduction over the cathode catalyst layer (in figure denoted as cathode activation), constitute almost 20–25% of the total irreversibilities, in low current densities. This is attributed to the fact that the oxygen reduction over the cathode catalyst is seriously hindered from the presence of the crossovered ethanol and the formation of I_p.

3.6. The effect of the oxygen feed concentration on cell performance and cathode activation overpotential

The effect of the oxygen feed concentration on the characteristic curves of the cell operation (*V–I* and *P–I*) is depicted in Fig. 8. From Fig. 8a, as the oxygen feed concentration increases, higher cell OCV values and improved cell discharge behavior is predicted. Higher oxygen concentration at the cathode side of the cell means higher oxygen partial pressure, leading consequently to more efficient fuel cell operation. Moreover, the combined effect of the anode mass transfer limitations (I_{lim}) and the slow anode electrochemical reaction, while the cathode is fed with high oxygen concentration, has as a consequence the limiting current to be strongly governed by the phenomena occurring at the anode side of the cell. However, in the case that the oxygen feed concentration is reduced 4.8 times (close to the ambient air composition) the mass transfer limitation (I_{lim}) is governed by the oxygen diffusivity at the cathode side of the cell for the base case values of the model parameters. Furthermore according to the model predictions regarding the cell power density presented in Fig. 8b the improved cell discharge behavior mentioned previously is depicted. Thus, as a conclusion, by increasing the oxygen feed concentration by 4.8 times the cell maximum power density is increased approximately 2.2 times from 13.5 mW cm^{-2} to 30.02 mW cm^{-2}.

The effect of the oxygen feed concentration at the cathode activation overpotential when the parasitic current is enabled and disabled is presented in Fig. 9. According to the model results, by increasing the oxygen concentration at the cathode side of the cell, the cathode activation overpotential is reduced for the base case values of the fuel cell operating parameters. This could be explained by the fact that the increase of oxygen concentration leads to: (a) higher oxygen concentrations at the cathode catalysts layer, thereby, leading to (b) higher electrochemical reaction rates at the cathode electrode.

Table 2
Overpotentials as a percentage (%) to the total overpotential for different operating current densities (model predictions) (cf. Fig. 7a)

Cell current density (mA cm^{-2})	Activation overpotential (%) ($\eta_a + \eta_{cath}$)	Ohmic overpotential (%) η_{ohmic}	Concentration overpotential (%) ($\eta_{conc,a} + \eta_{conc,cath}$)
5	93.382	0.525	6.093
10	93.327	0.899	5.774
20	92.498	1.55	5.952
40	90.463	2.66	6.877
80	86.359	4.467	9.174
120	82.256	5.896	11.848
160	77.838	6.944	15.218
180	75.402	7.207	17.391

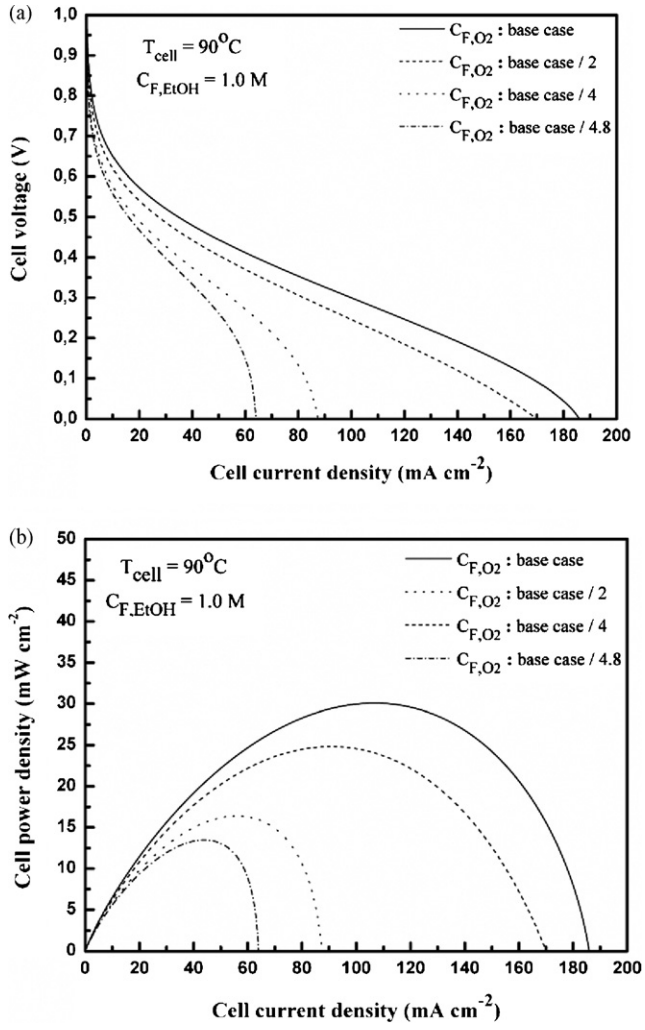

Fig. 8. (a) Direct Ethanol PEM Fuel Cell voltage–current density operation curves for different oxygen concentrations. (b) Direct Ethanol PEM Fuel Cell power density–current density operation curves for different oxygen concentrations.

3.7. The effect of parasitic current on DE-PEMFC operation

As, it was already mentioned, the term of the parasitic current (I_p), which is associated with the potential losses mostly due to ethanol crossover and the unwanted side reactions is needed to describe the operation of the fuel cell. In almost all PEM fuel cells, some current is lost due to these parasitic processes, even in the case of hydrogen PEMFCs. The net effect of this loss is to offset the fuel cell's operating current by an amount given by the term I_p. In other words, the fuel cell has to produce extra current to compensate for the current that is lost due to the parasitic effects. Schematically, these effects are depicted in Fig. 10. It is observed that among the most noticeable effects of the parasitic current is to reduce the fuel cell's open circuit voltage below its thermodynamically predicted value. Furthermore, the maximum cell power density value, which appears at midrange current densities, is strongly affected from the existence of the I_p. Additionally, at high operating current densities, the leakage current effects are also important. These observations are validated by a closer look of Eqs. (19), (22), (25) and (26).

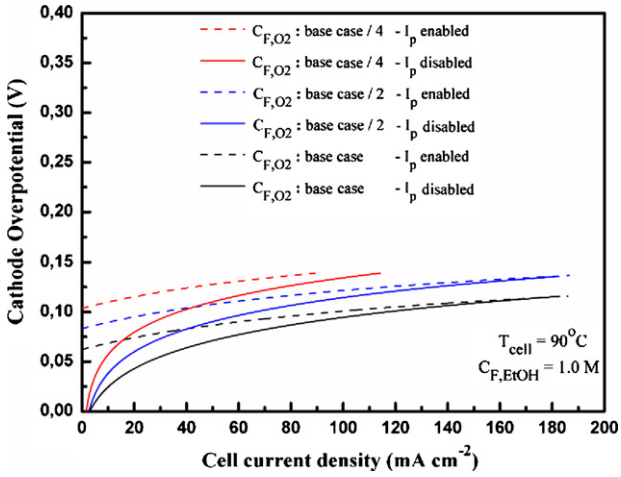

Fig. 9. Cathode overpotential vs. cell current density: I_p enabled–I_p disabled at different oxygen feed concentrations.

Finally, in Table 3, the effect of the unwanted current formation on the cell power density values is presented. The percentage of the cell power density losses is calculated from the cell power density predicted values, when I_p is enabled and disabled in the mathematical model equations. It is observed that the I_p formation affects the cell operation, no matter the operating cell current density. However, it seems that the highest losses (approximately 2.8 mW cm^{-2}) appear when the cell produces its highest power density value. In conclusion, from the mathematical model predictions, in a DE-PEMFC operating under the base case parameters' values an approximately 10.15% of power losses appears due to ethanol crossover that leads to the unwanted parasitic current formation. It is of great importance to note that when the cell is operated at 102 mA cm^{-2} (corresponds to the maximum power density value, when I_p is enabled) the power losses due to the parasitic current formation are approximately 9%. Finally, the maximum power density losses (75%) are found to be close to the limiting current density value. In the case of zero ethanol crossover the cell power den-

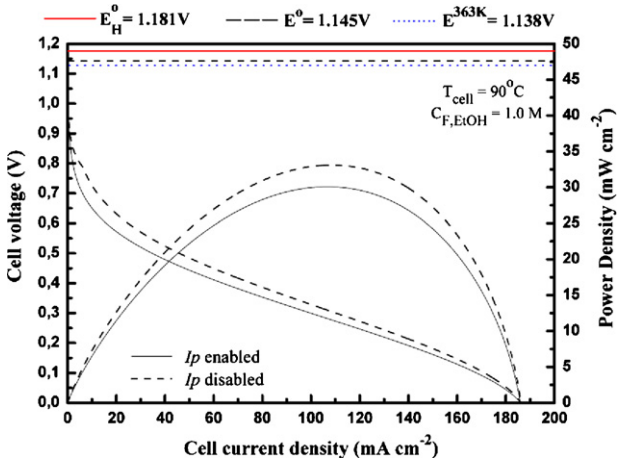

Fig. 10. The effect of the parasitic current (I_p) on the DE-PEMFC operation.

Table 3
Deviation between the results for the predicted cell power densities when the parasitic current is enabled and disabled in the mathematical model calculations, (mean value for the specified cell current density range)

Cell current density range ($mA\,cm^{-2}$)	Power density losses due to ethanol crossover (%)
[0–20]	9.25
[20–160]	9.22
[160–185]	15.62

sity is $0.8\,mW\,cm^{-2}$, while in the case of the I_p formation the corresponding power density value is equal to $0.2\,mW\,cm^{-2}$.

4. Conclusions

In the present work, a single-phase, 1-D mathematical model was developed with the purpose to describe the operation of a Direct Ethanol PEM Fuel Cell (DE-PEMFC) taking into account the negative effect of the parasitic current generation at the cathode side of the cell. Parasitic current (or leakage current) is the result of ethanol crossover from the anode to the cathode side of the cell passing through the polymer electrolyte membrane. According to the model results, at low ethanol feed concentrations, the ethanol crossover rate is reduced as the cell current density is increased resulting in lower values of parasitic current formation. In addition, the cathode activation overpotential when the parasitic current is enabled and disabled shows that the mixed overpotential of a DE-PEMFC poses a serious problem for the cell operation, especially when the cell is operated at low current density values. This is explained from the direct correlation existing between the ethanol crossover rate and the parasitic current formation. Furthermore, according to the irreversibilities ratio, resulting from the model predictions, it is proved that the main problems that DE-PEMFCs have to overcome are the slow kinetics of the ethanol electro-oxidation resulting to high anode activation overpotentials and the ethanol crossover hindering the oxygen reduction rate over the cathode catalyst. Moreover, it was found that the oxygen feed concentration (*oxygen partial pressure*) affects the cell operation, and less oxygen concentration at the cathode side reduces the total cell's power density. Finally, as it can be observed from the DE-PEMFC operation, when parasitic current is enabled in the mathematical model equations the most noticeable effects are: (a) the substantial reduction of the fuel cell's open circuit voltage and (b) the reduction of the fuel cell's discharge behavior.

Acknowledgement

This work is part of the 03ED897 research project, implemented within the framework of the "Reinforcement Programme of Human Research Manpower" (PENED) and co-financed by National and Community Funds (25% from the Greek Ministry of Development-General Secretariat of Research and Technology and 75% from EU-European Social Fund).

Appendix A

A.1. Thermodynamic calculations

Hereafter, the thermodynamic calculations concerning the thermo-neutral potential E_H° (corresponding to the ethanol's higher heating value HHV [65]), the theoretical potential E° and the Nernst potential E^{Nernst} of a DEFC are presented are as follows.

The thermo-neutral voltage of a direct ethanol fuel cell is calculated by:

$$E_H^\circ = -\frac{\Delta H^o}{zF} @ T_0 = 298\,K \Rightarrow E_H^\circ = 1.18145\,V \quad (a)$$

where $\Delta H^\circ = -1367.9\,kJ\,mol^{-1}$ [44] and corresponds to the HHV of ethanol (b).

The theoretical potential of a DEFC is calculated by:

$$E^\circ = -\frac{\Delta G^o}{zF} \;@\; T_0 = 298\,K \Rightarrow E^\circ = 1.14587\,V \quad (c)$$

where the value of ΔG° ($-1326.7\,kJ\,mol^{-1}$) is based on liquid water.

The Nernst potential is a function of the operating temperature and pressure and it is obtained by the following equation:

$$E^{Nernst} = E^\circ - \frac{RT}{zF}\ln\frac{(P_{CO_2}^2/P^\circ)(P_{H_2O}^3/P^\circ)}{(P_{EtOH}/P^\circ)(P^3/P^\circ)} \quad (d)$$

P_i are the partial pressures of the reaction's reactants and products and P° is the ambient pressure equal to the atmospheric in the present calculations. However when the partial pressures are unknown, the Van't Hoff equation can be used approximately well when the temperature difference is small [66]:

$$\frac{d\ln K}{dT} = \frac{\Delta H^\circ}{RT^2} \quad (e)$$

Also,

$$\Delta G = -RT\ln K \quad (f)$$

By integrating Eq. (e) and by combining it with Eq. (f) the following equation is formed:

$$\frac{\Delta G^{T_1}}{T_1} - \frac{\Delta G^{\circ T_0}}{T_0} = \Delta H^\circ\left(\frac{1}{T_1} - \frac{1}{T_0}\right) \quad (g)$$

T_1 is the operating temperature and ΔG^{T_1} the Gibbs energy at the specific operating temperature (T_1). In the present case, T_1 is equal to 363 K, thus Eq. (g) is formed as follows:

$$\frac{\Delta G^{363\,K}}{363} - \frac{\Delta G^\circ}{298} = -\Delta H^\circ\left(\frac{1}{363} - \frac{1}{298}\right) \Rightarrow \Delta G^{363\,K} = -1317.714\,kJ\,mol^{-1} \quad (h)$$

So, the Nernst potential at 363 K is:

$$E^{Nerst@363\,K} = -\frac{\Delta G^{363\,K}}{zF} \Rightarrow E^{Nerst@363\,K} = 1.13811\,V \quad (i)$$

Table A1
Error (%) between the model voltage predictions and the experimental results: Error (%) = $|(V^{model} - V^{exp})/V^{model}| \times 100\%$

Current density range (mA cm^{-2})	Error (%) mean value	
	Experiment #1	Experiment #2
[0–20]	4.95	9.3
[20–160]	4.10	6.43
[160–185]	14.60	9.83

A.2. Error percentage between the model results and the experimental data

See Table A1.

References

[1] S. Song, P. Tsiakaras, Appl. Catal. B: Environ. 63 (2006) 187–193.
[2] E. Antolini, J. Power Sources 170 (2007) 1–12.
[3] C. Lamy, S. Rousseau, E. Belgsir, C. Coutanceau, J. Leger, Electrochim. Acta 49 (2004) 3901–3908.
[4] S. Song, W. Zhou, J. Tian, R. Cai, G. Sun, Q. Xin, S. Kontou, P. Tsiakaras, J. Power Sources 145 (2005) 266–271.
[5] S. Song, Z. Liang, W. Zhou, G. Sun, Q. Xin, V. Stergiopoulos, P. Tsiakaras, J. Power Sources 145 (2005) 495–501.
[6] S. Kontou, V. Stergiopoulos, S. Song, P. Tsiakaras, J. Power Sources 171 (2007) 1–7.
[7] S. Song, V. Maragou, P. Tsiakaras, J. Fuel Cell Sci. Tech. 4 (2007) 203–209.
[8] W. Vielstich, A. Lamm, H. Gasteiger, Handbook of Fuel Cells, Fundamentals Technology and Applications, John Wiley press Inc., England, 2003.
[9] C. Lamy, A. Lima, V. LeRhun, F. Delime, C. Coutanceau, J. Leger, J. Power Sources 105 (2002) 283–296.
[10] Z. Wang, G. Yin, J. Zhang, Y. Sun, P. Shi, J. Power Sources 160 (2006) 37–43.
[11] W. Zhou, Z. Zhou, S. Song, W. Li, G. Sun, P. Tsiakaras, Q. Xin, Appl. Catal. B: Environ. 46 (2003) 273–285.
[12] X. Zhao, L. Jiang, G. Sun, S. Yang, B. Yi, X. Qin, Chin. J. Catal. 25 (2004) 983–988.
[13] E. Spinace, M. Linardi, A. Neto, Electrochem. Commun. 7 (2005) 365–369.
[14] F. Colmati, E. Antolini, E. Gonzalez, J. Power Sources 157 (2006) 98–103.
[15] F. Colmati, E. Antolini, E. Gonzalez, Appl. Catal. B: Environ. 73 (2007) 106–115.
[16] S. Rousseau, C. Coutanceau, C. Lamy, J. Leger, J. Power Sources 158 (2006) 18–24.
[17] E. Antolini, F. Colmati, E. Gonzalez, Electrochem. Commun. 9 (2007) 398–404.
[18] S. Song, Y. Wang, P. Tsiakaras, P.K. Shen, Appl. Catal. B: Environ. 78 (2008) 381–387.
[19] P.E. Tsiakaras, J. Power Sources 171 (2007) 107–112.
[20] S. Baxter, V. Battaglia, R. White, J. Electrochem. Soc. 146 (1999) 437–447.
[21] C. Chen, T. Yeh, J. Power Sources 160 (2006) 1131–1141.
[22] K. Jeng, C. Chen, J. Power Sources 112 (2002) 367–375.
[23] A. Kulikovsky, Electrochem. Commun. 5 (2003) 530–538.
[24] V. Oliveira, D. Falcao, C. Rangel, A. Pinto, Int. J. Hydrogen Energy 32 (2007) 415–424.
[25] S. Sandhu, R. Crowther, J. Fellner, Electrochim. Acta 50 (2005) 3985–3991.
[26] K. Scott, P. Argyropoulos, K. Sundmacher, J. Electroanal. Chem. 477 (1999) 97–110.
[27] K. Scott, W. Taama, J. Cruickshank, J. Power Sources 65 (1997) 159–171.
[28] K. Yin, J. Power Sources 167 (2007) 420–429.
[29] K. Sundmacher, T. Schultz, S. Zhou, K. Scott, M. Ginkel, E. Gilles, Chem. Eng. Sci. 56 (2001) 333–341.
[30] Z. Wang, C. Wang, J. Electrochem. Soc. 150 (2003) A508–A519.
[31] J. Meyers, J. Newman, J. Electrochem. Soc. 149 (2002) A718–A728.
[32] J. Meyers, J. Newman, J. Electrochem. Soc. 149 (2002) A710–A717.
[33] J. Meyers, J. Newman, J. Electrochem. Soc. 149 (2002) A729–A735.
[34] W. Yang, T. Zhao, J. Power Sources 174 (2007) 136–147.
[35] W. Yang, T. Zhao, Electrochim. Acta 52 (2007) 6125–6140.
[36] G. Andreadis, P. Tsiakaras, Chem. Eng. Sci. 61 (2006) 7497–7508.
[37] A. Podias, G. Andreadis, P. Tsiakaras, Single phase flow and Transport in Direct Ethanol Fuel Cells. 10th Grove Fuel Cells Symposium, 25–27 September 2007, London, UK, 2007.
[38] I. Sarris, P. Tsiakaras, S. Song, N. Vlachos, Solid State Ionics 177 (2006) 2133–2138.
[39] R. Rightmire, R. Rowland, D. Boos, D. Beals, J. Electrochem. Soc. 111 (1964) 242.
[40] T. Iwasita, B. Rasch, E. Cattaneo, W. Vielstich, Electrochim. Acta 34 (1989) 1073–1079.
[41] M. Watanabe, S. Motoo, J. Electroanal. Chem. 60 (1975) 267–273.
[42] W. Zhou, W. Li, S. Song, Z. Zhou, L. Jiang, G. Sun, Q. Xin, K. Poulianitis, S. Kontou, P. Tsiakaras, J. Power Sources 131 (2004) 217–223.
[43] W. Zhou, S. Song, W. Li, Z. Zhou, G. Sun, Q. Xin, S. Douvartzides, P. Tsiakaras, J. Power Sources 140 (2005) 50–58.
[44] C. Lamy, E. Belgsir, J. Leger, J. Appl. Electrochem. 31 (2001) 799–809.
[45] J. Wang, S. Wasmus, R. Savinell, J. Electrochem. Soc. 142 (1995) 4218–4224.
[46] Q. Wang, G. Sun, L. Cao, L. Jiang, G. Wang, S. Wang, S. Yang, Q. Xin, J. Power Sources 177 (2008) 142–147.
[47] F. Delime, J. Leger, C. Lamy, J. Appl. Electrochem. 28 (1997) 27–35.
[48] H. Hitmi, E. Belgsir, J. Leger, C. Lamy, R. Lezna, Electrochim. Acta 39 (1994) 407–415.
[49] A. Verma, S. Basu, J. Power Sources 168 (2007) 200–210.
[50] C. Marr, X. Li, J. Power Sources 77 (1999) 17–27.
[51] J. Liu, J. Ye, C. Xu, S. Jiang, Y. Tong, Electrochem. Commun. 9 (2007) 2334–2339.
[52] K. Jeng, C. Kuo, S. Lee, J. Power Sources 128 (2004) 145–151.
[53] K. Neyerlin, W. Gu, J. Jorne, H. Gasteiger, J. Electrochem. Soc. 153 (2006) A1955–A1963.
[54] A. Parthasarathy, C. Martin, S. Srinivasan, J. Electrochem. Soc. 138 (1991) 916–921.
[55] C. Du, T. Zhao, C. Xu, J. Power Sources 167 (2007) 265–271.
[56] C. Du, T. Zhao, W. Yang, Electrochim. Acta 52 (2007) 5266–5271.
[57] P. Kauranen, E. Skou, J. Electroanal. Chem. 408 (1996) 189–198.
[58] B. Garcia, V. Sethuraman, J. Weidner, R. White, R. Dougal, J. Fuel Cell Sci. Tech. 1 (2004) 43–48.
[59] A. Bard, L. Faulkner, Electrochemical Methods, Fundamentals and Applications, John Willey and Sons, New York, 2001, pp. 29–34.
[60] J. Smith, H. Van Ness, M. Abbott, Introduction to Chemical Engineering Thermodynamics, Mc-Graw Hill, Inc., 1996.
[61] Y. Cengel, M. Boles, Thermodynamics, An Engineering Approach, Mc-Graw Hill Companies, Inc., 1998.
[62] W. Press, S. Teukolsky, W. Vetterling, B. Flannery, Numerical Recipes 3rd Edition: The Art of Scientific Computing, Cambridge University Press, New York, 2002.
[63] D. Bernardi, M. Verbrugge, AIChE J. 37 (1991) 1151–1163.
[64] G. Naterer, C. Tokarz, J. Avsec, Int. J. Heat Mass Transfer 49 (2006) 2673–2683.
[65] N. Sammes, Fuel Cell Technology, Reaching Towards Commercialization, Springer Editions, Germany, 2006, pp. 29–30.
[66] J. Smith, Chemical Engineering Kinetics, Mc-Graw Hill, 1981.
[67] R. Reid, J. Prausnitz, B. Poling, The Properties of Gases & Liquids, Mc-Graw Hill International Editions, Chemical Engineering Series Inc., Singapore, 1988, pp. 581–586.
[68] F. Jaouen, G. Lindbergh, G. Sundholm, J. Electrochem. Soc. 149 (2002) A437–A447.
[69] A. Kulikovsky, Electrochem. Commun. 4 (2002) 939–946.
[70] S. Kato, K. Nagahama, H. Asai, J. Membr. Sci. 72 (1992) 31–41.
[71] X. Ren, W. Henderson, S. Gottesfeld, J. Electrochem. Soc. 144 (1997) L267–L270.
[72] T. Springer, T. Zawodzinski, S. Gottesfeld, J. Electrochem. Soc. 138 (1991) 2334–2342.